

Carboxylesterase-2-Selective Two-Photon Ratiometric Probe Reveals Decreased Carboxylesterase-2 Activity in Breast Cancer Cells

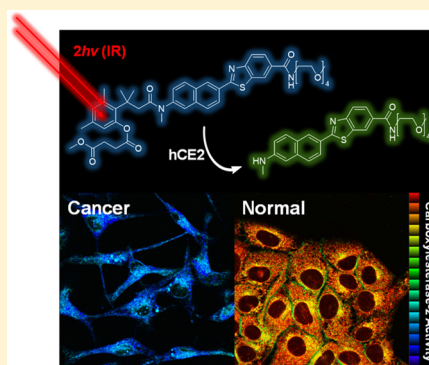
Sang Jun Park,[†] Yun Ji Kim,[†] Ji Su Kang,[†] In Young Kim,[‡] Kyeong Sook Choi,^{*,‡} and Hwan Myung Kim^{*,†}

[†]Department of Energy Systems Research, Ajou University, Suwon 443-749, Korea

[‡]Department of Biochemistry, Ajou University School of Medicine, BK21 Plus Program, Department of Biomedical Sciences, Ajou University School of Medicine, Suwon, Korea

Supporting Information

ABSTRACT: Human carboxylesterase-2 (CE2) is a carboxylesterase that catalyzes the hydrolysis of endogenous and exogenous substrates. Abnormal CE2 levels are associated with various cancers, and CE2 is a key mediator of anticancer prodrugs, including irinotecan. Here, we developed a two-photon ratiometric probe for detecting CE2 activity using succinate ester as a recognition site for CE2. The probe showed high selectivity to CE2, a clear emission color change, high photostability, and bright two-photon microscopy (TPM) imaging capability, allowing the quantitative detection of CE2 activity in live cells. Using TPM ratio analysis, we show for the first time that CE2 activity was much lower in breast cancer cells than in normal cells. In CE2 overexpression studies, cancer cells had a markedly enhanced sensitivity to the cytotoxic effect of irinotecan, corresponding well with the TPM ratio of the probe. These results may provide useful information for quantitatively measuring CE2 activity *in situ* and predicting the responsiveness to anticancer drugs.



Carboxylesterases (CEs, EC 3.1.1.1) are widely distributed throughout the body and catalyze the hydrolysis of esters, amides, thioesters, and carbamates.^{1,2} There are two major isoforms of carboxylesterases in humans, CE1 and CE2. They are heterogeneously distributed throughout the organs; CE1 levels greatly exceed CE2 levels in the liver, whereas only CE2 is present and highly expressed in the intestine.³ Previous studies have reported decreased CE2 expression levels in many tumor tissues.^{4,5} CE2 is downregulated in colorectal cancer, whereas decreased serum levels of CE2 have been detected in the early stage of ovarian cancer.⁶ In pancreatic cancer tissue, higher CE2 expression was reported compared with that in normal pancreatic tissue.⁷

CE2 plays crucial roles in the metabolic activation of many prodrugs.⁸ Among carboxylesterases, CE2 is the most efficient at activating the prodrug irinotecan into its active metabolite, SN-38,⁹ and as a result, CE2 is receiving increased attention because of its potential role in anticancer therapies for the treatment of different types of cancer, including colon carcinoma,¹⁰ malignant glioma,¹¹ multiple myeloma,¹² and pancreatic cancer.⁷ In particular, the overexpression of CE2 resulted in an enhanced efficacy of irinotecan for multiple myeloma.¹² In addition, CE2 activity is a critical contributor to the sensitivity to FOLFIRINOX therapy,⁷ which includes irinotecan as an active component, for pancreatic cancer. These results suggest that CE2 assessment may be used to define a subset of patients likely

to respond to irinotecan-based cancer therapy. However, data on the cellular levels of CE2, its underlying therapeutic mechanism, and side-effects are lacking.

Several common genetic variants of the CE2 gene have been found to influence drug metabolism and clinical outcomes.¹³ Although experimental techniques, such as immunoblotting,¹⁴ RT-PCR,¹⁵ and LC-MS,¹⁶ can be used to measure the protein or mRNA levels of CE2, they do not provide information on CE2 activity. To directly detect and quantitatively measure CE2 activity in a living cell, a technique using a fluorescent probe may be required. Fluorescent probes for detecting CEs have been recently reported.^{17–23} Among these, probes based on the benzoyl group as a reaction site show high selectivity for CE2 (Scheme 1) and respond to the activity of CE2 in living cells.^{20,22} However, most of the probes rely on fluorescence intensity changes in a single detection region, so it is difficult to quantitatively measure the enzyme activity. In addition, the use of excitation by short wavelength light can damage the samples and generate reactive species.

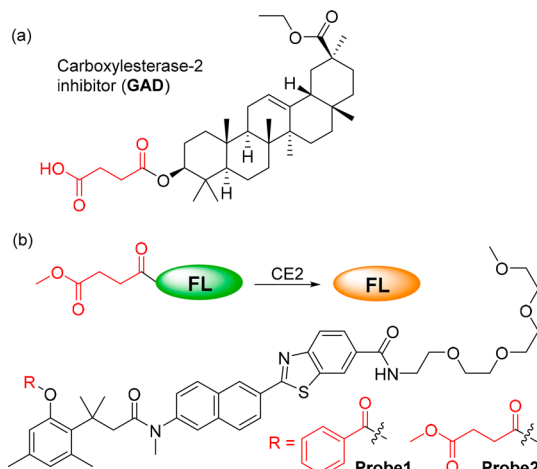
Two-photon microscopy (TPM) is a powerful tool for biomedical imaging. It uses two low-energy photons as an excitation source, minimizing damage to cells and tissues,

Received: May 10, 2018

Accepted: July 18, 2018

Published: July 18, 2018

Scheme 1. Structures of (a) 18 β -Glycyrrhetic Acid Derivative (GAD) as a CE2-Selective Inhibitor and (b) the Ratiometric Probes for CE2, Probe1 and Probe2



minimizing autofluorescence, and allowing high-quality images to be obtained over a long time period.^{24–30} In combination with TPM, a probe that changes its emission color in response to the activity of the enzyme would enable the analysis to be quantitative.^{31–41}

To generate a selective two-photon probe for CE2, we synthesized a benzoyl receptor-based probe, **Probe1** ([Scheme 1](#)). **Probe1** selectively reacts with CE2 and changes its emission color from blue to yellow. Unfortunately, this probe has a low photostability, which results in rapid decomposition of the benzoyl group under imaging conditions (see below). Therefore, we analyzed selective drugs and inhibitors for CE2 to find a reactive site that could replace the benzoyl group. We found a succinate ester-based prodrug (18β -glycyrhetic acid derivative), which showed a strong selective inhibitory effect on CE2 over CE1 ([Scheme 1a](#)).⁴² This led us to design a two-photon probe (**Probe2**) with succinate ester as the reaction site to CE2 ([Scheme 1b](#)).

Here, we developed a succinate ester-based, two-photon ratiometric probe, **Probe2**. The probe selectively responds to CE2 and changes its emission color from blue to yellow. **Probe2** has a very high photostability under imaging conditions, allowing CE2 activity to be precisely assessed in live cells. As CE2 is the main carboxylesterase in the human intestine, we first determined whether **Probe2** can be used to reliably measure CE2 activity in several types of colon cancer cells. In addition, we further assessed CE2 activity in normal breast cells and breast cancer cells, for which there is limited available information on CE2, using **Probe2** together with CE2 expression by immunoblot analysis. Our results show that the activity of CE2 in breast cancer cells is very low compared to that in normal cells. In addition, experiments using **Probe2** revealed that enhanced CE2 activity due to its overexpression makes breast cancer cells more vulnerable to the cytotoxicity of irinotecan.

■ EXPERIMENTAL SECTION

Enzymatic Kinetics Assays. Enzymatic kinetic assays were acquired using a Varioskan Flash micro plate reader with a 96-well plate. Various concentrations of **Probe1** and **Probe2** (0–60 μM) were prepared in PBS buffer solution (10 mM, pH 7.4). Human carboxylesterase enzyme was added to a concentration of 10 $\mu\text{g mL}^{-1}$, the fluorescence intensity was collected at 440

nm for **Probe1** and 455 nm for **Probe2**, respectively ($\lambda_{\text{ex}} = 373$ nm) with 37 °C. The initial rate (V_0) of the reaction was determined by using linear duration from 0 to 10 min (Figure S4 of the Supporting Information, SI). The Michaelis–Menten equation kinetic parameters were calculated with OriginPro 8.0.

Selectivity Assay. Each species (200 μ M ROS, 1 mM amino acids and glucose, 50 μ g mL $^{-1}$ BSA, 50 μ g mL $^{-1}$ HSA, 0.1% Human plasma, 10 μ g mL $^{-1}$ AChE, 10 μ g mL $^{-1}$ BChE, and 10 μ g mL $^{-1}$ hCE1 and hCE2) were administered to 1 μ M probes in PBS buffer (10 mM, pH 7.4), and the fluorescence spectra were measured as time. Amino acids (LAA21), glucose (G7528), bovine serum albumin (BSA, A2154), human serum albumin (HSA, A1653), human plasma (H4522), acetylcholinesterase (AChE, C2888, 1000 units mg $^{-1}$), butyrylcholinesterase (BChE, C7512, 10 units mg $^{-1}$), carboxylesterase 1 human (hCE1, E0287, 500 units mg $^{-1}$), and carboxylesterase 2 human (hCE2, E02, 500 units mg $^{-1}$) were purchased from Sigma-Aldrich.

Measurement of Two-Photon Cross Section. Probe1 and Probe2 (1.0×10^{-6} M) were dissolved in PBS containing 10% DMF, and the two-photon induced fluorescence intensity was acquired at 720–880 nm using rhodamine 6G as the reference. The TPA cross-section was calculated using $\delta = \delta_r(S_s\Phi_r\varphi_r c_r)/(S_r\Phi_s\varphi_s c_s)$, the subscripts s and r denote sample and reference molecules, respectively. The intensity of the signal measured by a CCD detector was denoted as S. Φ is the fluorescence quantum yield. φ is the fluorescence collection efficiency of the experimental equipment. c is the concentration of the molecules in solution. δ_r is the TPA cross-section of the reference molecule.

Cell Culture. All the cells were cultured on glass-bottomed dishes (NEST) and incubated in a humidified atmosphere of 5% CO₂ in air at 37 °C for 2 days before imaging. The cells were treated with 2 μM probes and incubated for 2 h, then they washed two times using serum-free media. Each cell culture mediums were supplemented with 10% FBS (WelGene), penicillin (100 units mL⁻¹), and streptomycin (100 μg mL⁻¹). The culture medium of RKO cells, HCT 116 cells, SW 837 cells, and MCF-7 cell is DMEM. The culture medium of MCF-10A cells is MEGM. The culture medium of MDA-MB 468 cells and MDA-MB 231 cells is RPMI1640.

Two-Photon Fluorescence Microscopy. Two-photon fluorescence microscopy images were obtained with multi-photon microscopes (Leica TCS SP8MP) with $\times 40$ oil objectives, numerical aperture (NA) = 1.30 by exciting the probes with a mode-locked titanium-sapphire laser source (Mai Tai HP) set at a wavelength of 740 nm and output power of 2490 mW, which corresponded to 4.14×10^8 mW cm $^{-2}$ average power in the focal plane.²⁶ To obtain images at 400–450 nm (F_{blue}) and 500–600 nm (F_{yellow}) range. Ratiometric image processing and analysis was carried out using MetaMorph software.

Photostability. Photostability of probes was determined by monitoring the changes in TPEF intensity with time at three designated positions of probe-labeled ($2.0 \mu\text{M}$) RKO cells chosen without bias (see below).

Western Blotting. Cells were washed in PBS buffer and lysed SDS-PAGE sample buffer (62.5 mM Tris-HCl, pH 6.8, 10% glycerol, 1% SDS and 5% β -mercaptoethanol). The lysates were heated for 5 min, separated by SDS-PAGE, and moved to an Immobilon membrane (Millipore, Bredford, MA, U.S.A.). After nonspecific binding sites blocking using 5% skim milk for 30 min, membranes were incubated with specific antibodies for

2 h. The following antibodies were used: CES2 (Santa Cruz biotechnology, Santa Cruz, CA, U.S.A.); β -actin, and Myc (Abcam, Cambridge, MA, U.S.A.). Then membranes were washed with TBST three times and further incubated for 1 h with horseradish peroxidase-conjugated antirabbit or antimouse antibody. Visualization of protein bands was accomplished using ECL (Advansta, Menlo Park, CA, U.S.A.). The each protein band intensity was quantified by densitometric analysis using the NIH ImageJ program. The fold change of protein levels compared to β -actin was verified by a densitometric analysis.

Overexpression of CE2 by Transfection. MDA-MB 468 and MDA-MB 231 cells were plated into 20 mm glass bottom cell culture dish at 1×10^5 cells/well. After 24 h, cells were transfected with the plasmid encoding CE2 (CES2 human tagged (MYC-DDK) ORF clone, OriGene Technologies, Rockville, MD, U.S.A.) using TransIT-2020 reagent (Mirus, San Diego, CA, U.S.A.) following the manufacturer's instruction. Transfected cells were incubated for 48 h and stained with Probe2. To further confirm the expression of CE2, Western blotting of the tagged MYC was performed.

Mesurement of Cell Viability. Cells (5×10^4 cells) were cultured in 24-well plates and treated with $10 \mu\text{mol L}^{-1}$ irinotecan for 24 h. For measurement of cellular viability, $2 \mu\text{mol L}^{-1}$ calcein-AM (Molecular Probe, Eugene, OR, U.S.A.), a green fluorescent indicator of the intracellular esterase activity of cells (live), and $4 \mu\text{mol L}^{-1}$ EthD-1 (Molecular Probe), a red fluorescent indicator of membrane-damaged cells (dead), were added to each well, and the plates were incubated for 5 min in $5\% \text{CO}_2$ at 37°C . Cells were then observed under a fluorescence microscope (Axiovert 200M; Carl Aeiss) equipped with Zeiss filter sets #46 and #64HE. Only exclusively green cells were counted as live. Each experiment was repeated at least three times. The percentage of live cells was normalized to that of untreated control cells (100%).

Statistical Analysis. All data are expressed as mean \pm SEM. Statistical analysis was performed using the Prism 5.03 software (GraphPad Prism, LaJolla CA, U.S.A.). Statistical differences were determined using a student *t* test. $p < 0.05$ was considered statistically significant.⁴³

RESULTS AND DISCUSSION

Probe1 and **Probe2** were synthesized by a coupling reaction between benzoyl or succinate ester containing a trimethyl lock moiety and BT DAN fluorophore (details in the SI). The spectroscopic properties of **Probe1** and **Probe2** were measured in PBS (10 mM, pH 7.4, 37°C , here and hereafter).

The solubilities of **Probe1** and **Probe2** in PBS were determined by a fluorescence titration method. The values were approximately 1 and 2 μM , respectively, which were sufficient to stain the cells (Figure S1). **Probe2** emitted a strong blue fluorescence with a maximum fluorescence wavelength of 455 nm in the buffer (fluorescence efficiency, 0.57). When hCE2 was added, the fluorescence of **Probe2** gradually shifted to a longer wavelength range (maximum fluorescence wavelength 540 nm, Figure 1c). These results may be due to the rapid elimination of the trimethyl lock linker after the enzymatic reaction (Schemes 1b and S2). As a result, the reacted form containing a strong electron donor is produced, so the intramolecular charge transfer character is enhanced. **Probe1** showed similar characteristics (Figure 1a). The detailed spectral data of **Probe1** and **Probe2** are summarized in Figure S2 and Table S1.

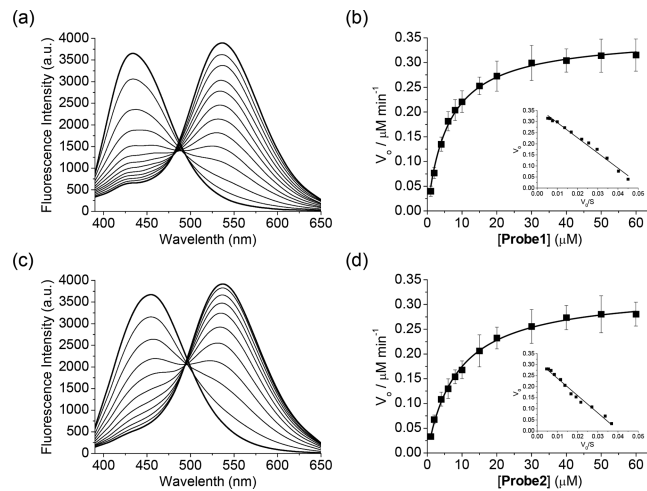


Figure 1. Enzymatic reaction of **Probe1** and **Probe2** with hCE2 fluorescence spectra of (a) **Probe1** ($1.0 \mu\text{M}$) and (c) **Probe2** ($1.0 \mu\text{M}$) in PBS before and after the addition of $10 \mu\text{g mL}^{-1}$ hCE2, measured every 120 s. Plot of V_0 versus the concentration of (b) **Probe1** and (d) **Probe2** after addition of $10 \mu\text{g mL}^{-1}$ hCE2 with 60 s intervals from 0 to 10 min. (inset) The corresponding Eadie-Hofstee plot. V_0 is the initial rate of reaction where S is the probes concentration. The excitation wavelength was 373 nm.

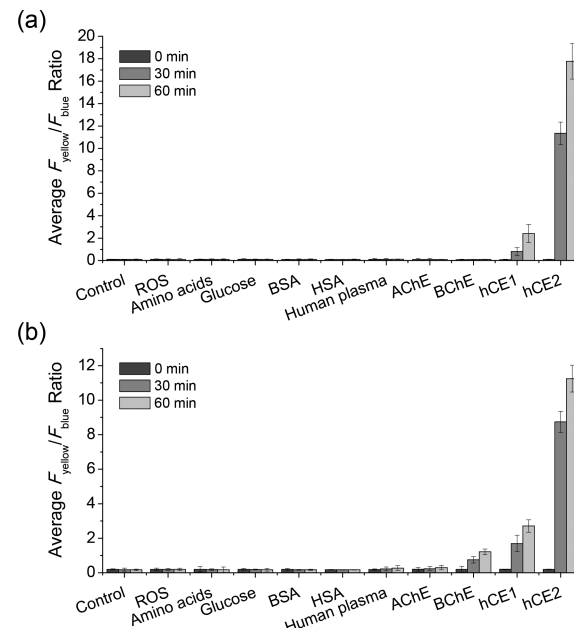


Figure 2. **Probe1** and **Probe2** selectivity experiments. Fluorescence responses of (a) **Probe1** ($1.0 \mu\text{M}$) and (b) **Probe2** ($1.0 \mu\text{M}$) to ROS (H_2O_2 , TBHP, OCl^- , O_2^- , NO, $\bullet\text{O}'\text{Bu}$, $\bullet\text{OH}$, ONOO^-), amino acids (Gly, Ala, Val, Cys, Pro, Leu, Ile, Met, Trp, Phe, Ser, Thr, Tyr, Asn, Glu, Lys, Arg, His, Asp, Glu), glucose, BSA, HSA, human plasma, AChE, BChE, hCE1, and hCE2. Bars represent the integrated fluorescence ratios ($F_{\text{yellow}}/F_{\text{blue}}$) 0 to 1 h after the addition of each species. The excitation wavelength was 373 nm.

The selectivity of the probes to CE2 was examined. The ratio ($F_{\text{yellow}}/F_{\text{blue}}$) of **Probe2** in the range of 420–470 nm (F_{blue}) and 520–570 nm (F_{yellow}) increased 70 times when CE2 was added (Figure 2). Alternatively, after the addition of CE1, the spectral changes of **Probe2** were very small. The kinetic behavior of reaction-based probe with enzyme gives important information for the quantitative applications.^{44–46} The enzymatic reaction

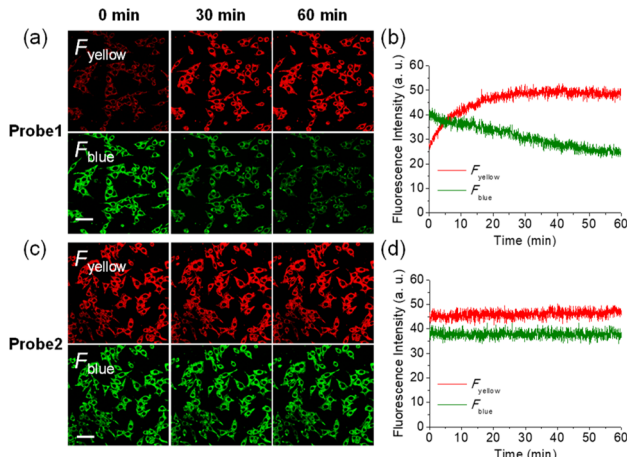


Figure 3. Probe behavior over time (a, c) TPM images ($F_{\text{yellow}}/F_{\text{blue}}$) of RKO cells labeled with (a) **Probe1** and (c) **Probe2** at different time points. (b, d) The relative TPEF intensity from panels a and c as a function of time. The digitized intensities were recorded at 2.00 s intervals for 1 h using xyt mode. Images were acquired using 740 nm excitation and emission windows of 400–450 nm (blue) and 500–600 nm (yellow) with femto-second pulses. Scale bars = 50 μm .

rate of **Probe2** was calculated according to the Michaelis–Menten method and confirmed by the corresponding Eadie–Hofstee plots (Figures 1 and S3). The apparent specificity constant for CE2 of **Probe2** was $k_{\text{cat}}/K_m = 3.8 \times 10^3 \text{ M}^{-1} \text{ s}^{-1}$, where $K_m = 8.8 \pm 0.4 \mu\text{M}$ (Figure 1 and Table S2), and the calculated value in the change interval of hCE1 was smaller (Figure S3 and Table S3). These results indicate that **Probe2** is preferred for CE2 over CE1, which is consistent with the previous result that the reaction site of the CE2 inhibitor (GAD) is succinate ester. The plot of the $F_{\text{yellow}}/F_{\text{blue}}$ versus the hCE2 concentration ranging from 0 to 170 nM showed a linear relationship (Figure S5), indicating that **Probe2** can detect hCE2 at concentrations as low as 7.7 nM. Subsequently, a selectivity test with other bioactive species was carried out. **Probe2** was not sensitive to ROS, amino acids, sugar, and metal ions, and other hydrolytic enzymes such as bovine serum albumin (BSA), human serum albumin (HSA), human plasma, acetylcholinesterase (AChE), and butyrylcholinesterase (BChE) also showed weak responses under the same amount ($10 \mu\text{g mL}^{-1}$) and activity (5 units mL^{-1}) conditions (Figure 2 and S6). To confirm these results, we further carried out inhibition assays in homogenized MCF-10A cells by using selective esterase inhibitors (Figure S7). Upon treatment with bis(4-nitrophenyl) phosphate (BNPP, a well-known inhibitor for CEs)⁴⁷ and loperamide (LPA, inhibitor for CE2),⁴⁸ the enzymatic reaction of **Probe2** was mostly suppressed, but not with other inhibitors for AChE, BChE, PON1, and PON2. **Probe2** was stable over a wide pH range (Figure S8). Similar trends were also observed for **Probe1** (Figures 2 and S5–S8).

Next, we tested the two-photon microscope imaging capabilities of the probes for CE2 employing RKO colon cancer cells, as CE2, but not CE1, was reported to be highly expressed in the intestine.³ Live RKO cells were stained with the probe and observed with a two-photon excitation source at 740 nm. The images were observed in the incubating chamber to maintain the temperature (37 °C), humidity (90%), and CO₂ (5%) at constant levels. A clear TPM image was obtained, probably because the probe stained cells well and had a sufficient two-photon action cross-section efficiency (15–72 GM, Figure S9).

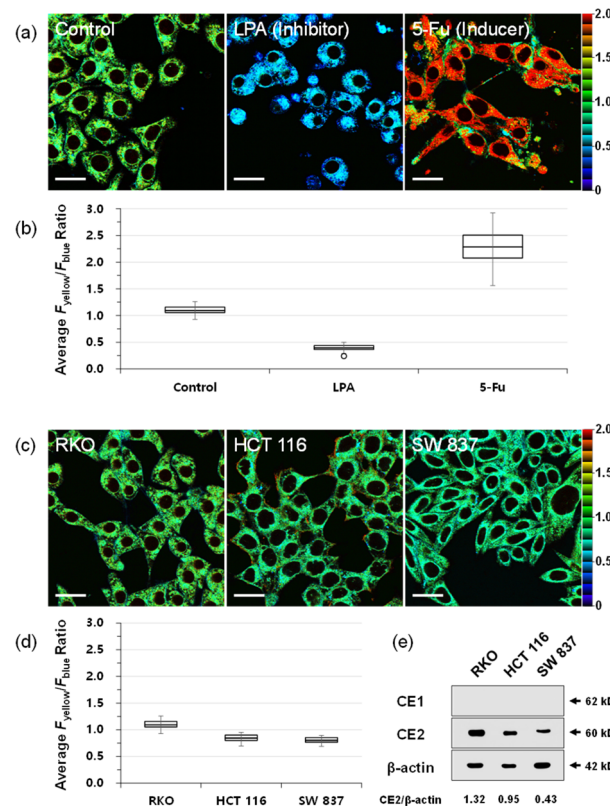


Figure 4. Pseudocolored ratiometric TPM images ($F_{\text{yellow}}/F_{\text{blue}}$) of colon cancer cells labeled with **Probe2** (2.0 μM). (a) Pseudocolored ratiometric TPM images ($F_{\text{yellow}}/F_{\text{blue}}$) of RKO cells labeled with **Probe2** for 2 h; cells were pretreated with loperamide (LPA, 100 μM) for 20 min and 5-fluorouracil (5-Fu, 10 μM) for 48 h before labeling with **Probe2**. (c) Pseudocolored ratiometric TPM images ($F_{\text{yellow}}/F_{\text{blue}}$) of RKO, HCT 116, and SW 837 cells labeled with **Probe2** for 2 h. (b, d) Average $F_{\text{yellow}}/F_{\text{blue}}$ intensity ratios in the TPM images. Images were acquired using 740 nm excitation and emission windows of 400–450 nm (blue) and 500–600 nm (yellow). Scale bars = 25 μm . (e) Western blot analysis of CE1 and CE2. The band intensity of CE2 was normalized to the respective β -actin band.

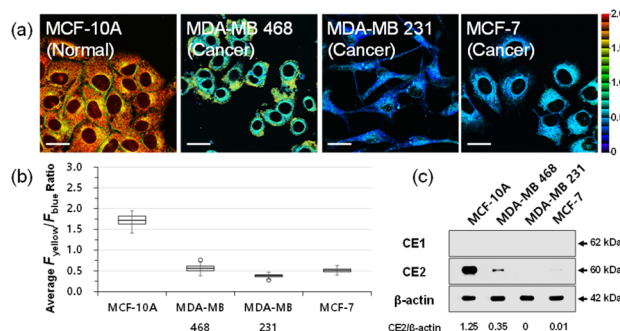


Figure 5. Pseudocolored ratiometric TPM images ($F_{\text{yellow}}/F_{\text{blue}}$) of breast cells labeled with **Probe2** (2.0 μM). (a) Pseudocolored ratiometric TPM images ($F_{\text{yellow}}/F_{\text{blue}}$) of MCF-10A, MDA-MB 468, MDA-MB 231, and MCF-7 cells labeled with **Probe2** for 2 h. (b) Average $F_{\text{yellow}}/F_{\text{blue}}$ intensity ratios in the TPM images. Images were acquired using 740 nm excitation and emission windows of 400–450 nm (blue) and 500–600 nm (yellow). Scale bars = 25 μm . (c) Western blot analysis of CE1 and CE2. The band intensity of CE2 was normalized to the respective β -actin band.

CCK-8 assays were also used to confirm that the probe had negligible cytotoxicity under imaging conditions (Figure S10).

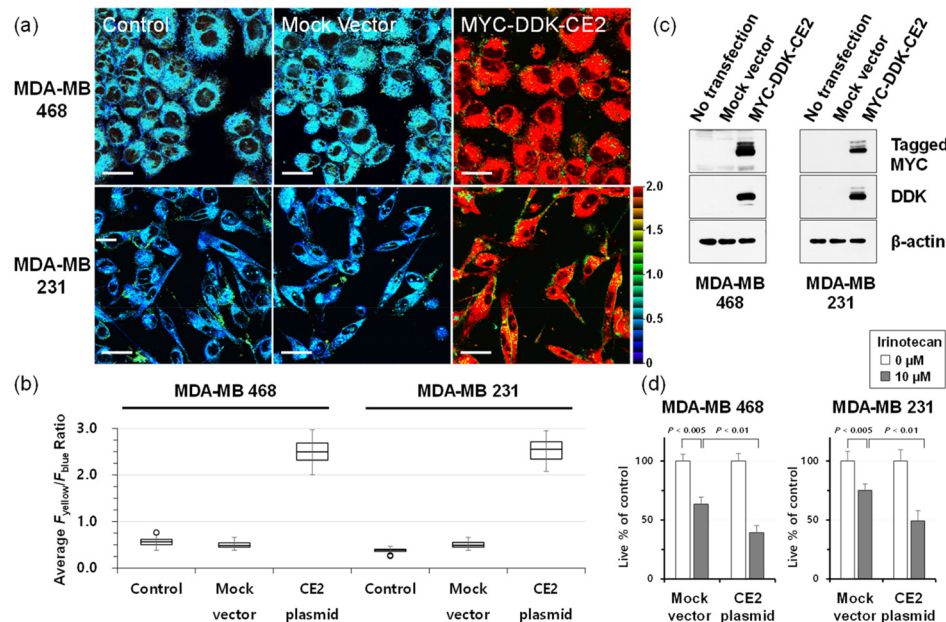


Figure 6. Overexpression of CE2 in breast cancer cells increases the TPM ratio of CE2 and enhances their sensitivity to irinotecan. (a–c) MDA-MB 468 and MDA-MB 231 cells were transfected with the mock vector or MYC-DDK-tagged CE2 plasmid for 24 h. (a) Transfected cells were further treated with **Probe2** for 2 h. Pseudocolored ratiometric TPM images ($F_{\text{yellow}}/F_{\text{blue}}$) of cells after transfection are shown. (b) Average $F_{\text{yellow}}/F_{\text{blue}}$ intensity ratios in the TPM images. Images were acquired using 740 nm excitation and emission windows of 400–450 nm (blue) and 500–600 nm (yellow). Scale bars = 25 μm . (c) Cell extracts were prepared after transfection, and Western blot analysis of Myc and β -actin was performed. (d) MDA-MB 468 cells transfected with the mock vector or CE2 plasmid were further treated with 10 μM for 24 h, and cellular viability was measured.

Green (400–450 nm, F_{green}) and yellow (500–600 nm, F_{yellow}) regions were selected as appropriate detection regions for the ratio images ($F_{\text{yellow}}/F_{\text{blue}}$). Fluorescence intensities were continuously recorded every 2 s to measure the photostability of the probes (Figure 3). The fluorescence intensity of **Probe2** was almost constant, possibly reflecting the strong photostability and fast enzyme response behavior observed in the cuvette. **Probe1**, however, appeared unstable: a fluorescence increase in F_{yellow} along with a decrease in F_{green} over time (Figure 3a). Similar results were observed in PBS buffer (Figure S11). These results indicate that **Probe2** is suitable for two-photon microscopy images, and further experiments were conducted using **Probe2**.

Then, we tested whether measurement of CE2 activity using **Probe2** could represent the changes in its activity in live cells treated with an inhibitor or inducer of CE2. Two-photon images taken after staining RKO colon cancer cells with **Probe2** revealed the presence of the probe throughout the cells except for the nucleus. Their average ratio value was calculated to be 1.09 (Figure 4a). After treatment with loperamide LPA and 5-fluorouracil (5-Fu, an inducer of CE2),¹⁵ the ratio values changed to 0.48 and 2.28, respectively (Figure 4b). Similar results were found in HCT 116 cells (Figure S12). These results suggest that the TPM results using **Probe2** could accurately represent the changes in CE2 activity in live cells in response to an inhibitor or activator. Next, we compared the TPM results with Western blotting results using specific antibodies against CE1 and CE2 in several colon cancer cell lines. Measurement of CE2 activity using **Probe2** revealed that the ratio value was higher in RKO cells than in HCT 116 cells and was the lowest in SW 837 cells (Figure 4d). Western blot analysis of CE2 also showed that the order of CE2 protein levels in the colon cancer cell lines was RKO > HCT 116 > SW 837 cells (Figure 4e), showing a very good correlation between the **Probe2**-based CE2

activity and CE2 protein levels in these colon cancer cells (Figure 4d, e). The expression of CE1 was not detected, consistent with a previous report that only CE2 is highly expressed in the intestine.³ These results indicate the potential applicability of **Probe2** as a reliable tool to measure CE2 activity in other types of cancer.

Compared to other types of cancers, information on CE2 expression and activity in breast cells is quite limited. Therefore, we next determined whether **Probe2** could be used to fill this information gap and assess CE2 activity in breast cancer cells and normal breast cells. We found that although the TPM ratio of **Probe2** was markedly high (1.72) in MDA-10A normal breast cells, it was much lower in the tested breast cancer cells, MDA-MB 468, MDA-MB 231, and MCF-7 cells (Figure 5a, b). These results suggest that CE2 activity in breast cancer cells may be much lower than that in their normal counterpart cells. Western blot analysis also revealed very high protein levels of CE2 in MCF-10A cells, but CE2 was very weakly expressed in MDA-MB 468 cells (Figure 5c). In MDA-MB 231 and MCF-7 cells, we were unable to detect CE2 protein levels (Figure 5c). These results indicate that CE2 activity, measured using **Probe2**, shows a good correlation with its protein level in these breast cells. In addition, the TPM ratio of **Probe2** was reduced after treating MDA-MB 468 cells with LPA but markedly increased by 5-FU (Figure S12), showing that **Probe2** accurately reflects the changes in CE2 activity in these breast cancer cells following treatment with these pharmacological modulators of CE2.

The potential applicability of **Probe2** as a reliable tool to measure CE2 activity was further confirmed by exogenously expressing CE2 in breast cancer cells whose endogenous CE2 protein levels are low. Transfection with a plasmid encoding Myc-DDK-tagged CE2, but not with the mock vector, dramatically increased not only the activity but also the protein level of CE2 in both MDA-MB 468 and MDA-MB 231 cells

(Figure 6a–c). As an inverse relationship between CE2 activity and half-maximal inhibitory concentration (IC_{50}) of irinotecan was reported in pancreatic cancer cells,⁷ we further tested whether the forced expression of CE2 could enhance the sensitivity of breast cancer cells to irinotecan. We transfected MDA-MB 468 and MDA-MB-231 cells with an Myc-DDK-tagged CE2 plasmid and then treated them with 10 μ M irinotecan for 24 h. Measurement of cell viability showed that irinotecan-mediated cell death was significantly enhanced by CE2 overexpression in these cells (Figure 6d). These results suggest that **Probe2** may have potential applicability as a tool to predict the responsiveness of cancer patients to irinotecan-based cancer therapy.

To the best of our knowledge, this is the first evidence that the protein levels and activities of CE2 are significantly lower in breast cancer cells than in normal cells. In addition, we clearly show that **Probe2** is useful for directly detecting and quantitatively assessing the differences in CE2 activity in biological samples. The use of **Probe2** as a tool to easily and accurately measure CE2 activity in solid tumors may provide valuable information to improve the clinical outcomes of irinotecan treatment and avoid its potential side effects. To improve the potential application of **Probe2** in personalized medicine, further studies employing patient-derived xenograft models are warranted.

CONCLUSIONS

We developed a succinate ester-based, two-photon ratiometric probe (**Probe2**) for the detection of CE2 activity. The probe selectively responds to CE2 and shows a clear blue-to-yellow emission color change under physiological conditions. **Probe2** is highly photostable, is easily loaded into cells, and can be used to produce bright two-photon microscopy (TPM) images for quantitatively analyzing CE2 activity in live cells. Using TPM ratiometric analysis, we show here for the first time that CE2 activity is much lower in breast cancer cells than in normal cells. In addition, we demonstrate that CE2 overexpression in breast cancer cells increases CE2 activity and the sensitivity to irinotecan. These results provide useful information for quantitatively measuring CE2 activity and predicting the responsiveness to anticancer drugs.

ASSOCIATED CONTENT

Supporting Information

The Supporting Information is available free of charge on the ACS Publications website at DOI: [10.1021/acs.analchem.8b02101](https://doi.org/10.1021/acs.analchem.8b02101).

Synthesis of **Probe1** and **Probe2**; spectroscopic measurements; water solubility; enzymatic kinetics assays; inhibitor assays; measurement of two-photon cross section; cell viability; and photostability (Figures S1–S34 and Tables S1–S3) ([PDF](#))

AUTHOR INFORMATION

Corresponding Authors

*Fax: +82-31-219-1615. E-mail: kimhm@ajou.ac.kr.

*E-mail: kschoi@ajou.ac.kr.

ORCID

Hwan Myung Kim: [0000-0002-4112-9009](#)

Notes

The authors declare no competing financial interest.

ACKNOWLEDGMENTS

This study was supported by grant from the National Leading Research Lab Program of the National Research Foundation of Korea (NRF) funded by the Korean government (MSIP) (No. 2016R1E1A1A02920873). K.S.C. acknowledges a grant from the NRF (No. 2011-0030043).

REFERENCES

- (1) Satoh, T.; Hosokawa, M. *Annu. Rev. Pharmacol. Toxicol.* **1998**, *38*, 257–288.
- (2) Laizure, S. C.; Herring, V.; Hu, Z.; Witbrodt, K.; Parker, R. B. *Pharmacotherapy* **2013**, *33*, 210–222.
- (3) Imai, T.; Taketani, M.; Shii, M.; Hosokawa, M.; Chiba, K. *Drug Metab. Dispos.* **2006**, *34*, 1734–1741.
- (4) Tang, X.; Wu, H.; Wu, Z.; Wang, G.; Wang, Z.; Zhu, D. *Cancer Invest.* **2008**, *26*, 178–181.
- (5) Yu, J.; Li, X.; Zhong, C.; Li, D.; Zhai, X.; Hu, W.; Guo, C.; Yuan, Y.; Zheng, S. *Oncotarget* **2016**, *7*, 75279–75292.
- (6) Cai, L.; Tang, X.; Guo, L.; An, Y.; Wang, Y.; Zheng, J. *Tumori* **2009**, *95*, 473–478.
- (7) Capello, M.; Lee, M.; Wang, H.; Babel, I.; Katz, M. H.; Fleming, J. B.; Maitra, A.; Wang, H.; Tian, W.; Taguchi, A.; Hanash, S. M. *J. Natl. Cancer Inst.* **2015**, *107*, 107.
- (8) Wang, D. D.; Zou, L. W.; Jin, Q.; Hou, J.; Ge, G. B.; Yang, L. *Fitoterapia* **2017**, *117*, 84–95.
- (9) Xu, G.; Zhang, W.; Ma, M. K.; McLeod, H. L. *Clin. Cancer Res.* **2002**, *8*, 2605–2611.
- (10) Oosterhoff, D.; Pinedo, H. M.; van der Meulen, I. H.; de Graaf, M.; Sone, T.; Kruyt, F. A.; van Beusechem, V. W.; Haisma, H. J.; Gerritsen, W. R. *Br. J. Cancer* **2002**, *87*, 659–664.
- (11) Tymianski, E.; Leroy, S.; Terada, K.; Finkelstein, D. M.; Hyatt, J. L.; Danks, M. K.; Potter, P. M.; Saeki, Y.; Chiocca, E. A. *Cancer Res.* **2005**, *65*, 6850–6857.
- (12) Yano, H.; Kayukawa, S.; Iida, S.; Nakagawa, C.; Oguri, T.; Sanda, T.; Ding, J.; Mori, F.; Ito, A.; Ri, M.; Inagaki, A.; Kusumoto, S.; Ishida, T.; Komatsu, H.; Inagaki, H.; Suzuki, A.; Ueda, R. *Cancer Sci.* **2008**, *99*, 2309–2314.
- (13) Merali, Z.; Ross, S. C.; Paré, G. *Drug Metab. Drug Interact.* **2014**, *29*, 143–151.
- (14) Godin, S. J.; Crow, J. A.; Scollon, E. J.; Hughes, M. F.; DeVito, M. J.; Ross, M. K. *Drug Metab. Dispos.* **2007**, *35*, 1664–1671.
- (15) Choi, W.; Cogdell, D.; Feng, Y.; Hamilton, S. R.; Zhang, W. *Cancer Biol. Ther.* **2006**, *5*, 1450–1456.
- (16) Sato, Y.; Miyashita, A.; Iwatsubo, T.; Usui, T. *Drug Metab. Dispos.* **2012**, *40*, 1389–1396.
- (17) Chandran, S. S.; Dickson, K. A.; Raines, R. T. *J. Am. Chem. Soc.* **2005**, *127*, 1652–1653.
- (18) Wang, J.; Williams, E. T.; Bourgea, J.; Wong, Y. N.; Patten, C. J. *Drug Metab. Dispos.* **2011**, *39*, 1329–1333.
- (19) Lavis, L. D.; Chao, T.; Raines, R. T. *Chem. Sci.* **2011**, *2*, 521–530.
- (20) Feng, L.; Liu, Z. M.; Xu, L.; Lv, X.; Ning, J.; Hou, J.; Ge, G. B.; Cui, J. N.; Yang, L. *Chem. Commun.* **2014**, *50*, 14519–14522.
- (21) Jin, Q.; Feng, L.; Wang, D. D.; Dai, Z. R.; Wang, P.; Zou, L. W.; Liu, Z. H.; Wang, J. Y.; Yu, Y.; Ge, G. B.; Cui, J. N.; Yang, L. *ACS Appl. Mater. Interfaces* **2015**, *7*, 28474–28481.
- (22) Jin, Q.; Feng, L.; Wang, D. D.; Wu, J. J.; Hou, J.; Dai, Z. R.; Sun, S. G.; Wang, J. Y.; Ge, G. B.; Cui, J. N.; Yang, L. *Biosens. Bioelectron.* **2016**, *83*, 193–199.
- (23) Park, S. J.; Lee, H. W.; Kim, H. R.; Kang, C.; Kim, H. M. *Chem. Sci.* **2016**, *7*, 3703–3709.
- (24) Helmchen, F.; Denk, W. *Nat. Methods* **2005**, *2*, 932–940.
- (25) Kim, H. M.; Cho, B. R. *Acc. Chem. Res.* **2009**, *42*, 863–872.
- (26) Kim, H. M.; Cho, B. R. *Chem. Rev.* **2015**, *115*, 5014–5055.
- (27) Qian, L.; Li, L.; Yao, S. Q. *Acc. Chem. Res.* **2016**, *49*, 626–634.
- (28) Tang, Y.; Kong, X.; Xu, A.; Dong, B.; Lin, W. *Angew. Chem., Int. Ed.* **2016**, *55*, 3356–3359.
- (29) Mao, Z.; Jiang, H.; Li, Z.; Zhong, C.; Zhang, W.; Liu, Z. *Chem. Sci.* **2017**, *8*, 4533–4538.

- (30) Qian, J.; Zhu, Z.; Leung, C. W.; Xi, W.; Su, L.; Chen, G.; Qin, A.; Tang, B. Z.; He, S. *Biomed. Opt. Express* **2015**, *6*, 1477–1486.
- (31) Brewer, T. F.; Burgos-Barragan, G.; Wit, N.; Patel, K. J.; Chang, C. J. *Chem. Sci.* **2017**, *8*, 4073–4081.
- (32) Lim, C. S.; Masanta, G.; Kim, H. J.; Han, J. H.; Kim, H. M.; Cho, B. R. *J. Am. Chem. Soc.* **2011**, *133*, 11132–11135.
- (33) Zhang, H.; Fan, J.; Wang, J.; Dou, B.; Zhou, F.; Cao, J.; Qu, J.; Cao, Z.; Zhao, W.; Peng, X. *J. Am. Chem. Soc.* **2013**, *135*, 17469–17475.
- (34) Lee, M. H.; Sharma, A.; Chang, M. J.; Lee, J.; Son, S.; Sessler, J. L.; Kang, C.; Kim, J. S. *Chem. Soc. Rev.* **2018**, *47*, 28–52.
- (35) Kim, H. J.; Lim, C. S.; Lee, H. W.; Lee, H. S.; Um, Y. J.; Kumar, H.; Han, I.; Kim, H. M. *Biomaterials* **2017**, *141*, 251–259.
- (36) Jun, Y. W.; Sarkar, S.; Singha, S.; Reo, Y. J.; Kim, H. R.; Kim, J. J.; Chang, Y. T.; Ahn, K. H. *Chem. Commun.* **2017**, *53*, 10800–10803.
- (37) Xie, X.; Fan, J.; Liang, M.; Li, Y.; Jiao, X.; Wang, X.; Tang, B. *Chem. Commun.* **2017**, *53*, 11941–11944.
- (38) Wu, D.; Chen, L.; Lee, W.; Ko, G.; Yin, J.; Yoon, J. *Coord. Chem. Rev.* **2018**, *354*, 74–97.
- (39) Youssef, S.; Ren, W.; Ai, H. W. *ACS Chem. Biol.* **2016**, *11*, 2492–2498.
- (40) Sun, X.; James, T. D. *Chem. Rev.* **2015**, *115*, 8001–8037.
- (41) Chen, Y.; Bai, Y.; Han, Z.; He, W.; Guo, Z. *Chem. Soc. Rev.* **2015**, *44*, 4517–4546.
- (42) Zou, L. W.; Li, Y. G.; Wang, P.; Zhou, K.; Hou, J.; Jin, Q.; Hao, D. C.; Ge, G. B.; Yang, L. *Eur. J. Med. Chem.* **2016**, *112*, 280–288.
- (43) Dahiru, T. *Ann. Ib. Postgrad. Med.* **2008**, *6*, 21–26.
- (44) Ge, G. B.; Ning, J.; Hu, L. H.; Dai, Z. R.; Hou, J.; Cao, Y. F.; Yu, Z. W.; Ai, C. Z.; Gu, J. K.; Ma, X. C.; Yang, L. *Chem. Commun.* **2013**, *49*, 9779–9781.
- (45) Jin, Q.; Feng, L.; Zhang, S. J.; Wang, D. D.; Wang, F. J.; Zhang, Y.; Cui, J. N.; Guo, W. Z.; Ge, G. B.; Yang, L. *Anal. Chem.* **2017**, *89*, 9884–9891.
- (46) Dai, Z. R.; Feng, L.; Jin, Q.; Cheng, H.; Li, Y.; Ning, J.; Yu, Y.; Ge, G. B.; Cui, J. N.; Yang, L. *Chem. Sci.* **2017**, *8*, 2795–2803.
- (47) Siebert, H.; Engelke, S.; Maruschak, B.; Bruck, W. *Brain Res.* **2001**, *916*, 159–164.
- (48) Quinney, S. K.; Sanghani, S. P.; Davis, W. I.; Hurley, T. D.; Sun, Z.; Murry, D. J.; Bosron, W. F. *J. Pharmacol. Exp. Ther.* **2005**, *313*, 1011–1016.